Towards the Development of Tactile Sensors for Surface Texture Detection

Moritz Scharff, Carsten Behn
Technical Mechanics Group
Department of Mechanical Engineering
Technische Universität Ilmenau
Max-Planckring 12
98693 Ilmenau, Germany
Email: Moritz.Scharff@TU-Ilmenau.de

Joachim Steigenberger
Institute of Mathematics
Technische Universität Ilmenau

Jorge Alencastre
Department of Engineering
Section Mechanical Engineering
Pontifical Catholic University of Peru

***Abstract*—Adapting the principle of natural vibrissae, artificial tactile sensors are designed to fulfill the functions: object distance detection, object shape recognition and surface texture scanning. To realize the process of surface texture detection with an artificial sensor, firstly a theoretical approach is done. Replacing the natural vibrissa by an Euler-Bernoulli bending beam and modeling the vibrissa-surface contact with respect to Coulomb's Law of Friction, a quasi-static scenario is performed. In this, the support of the vibrissa moves in a way that the tip of the beam gets pushed. Starting the movement of the support, the tip of the beam is sticking to the surface until the maximal stiction force is reached. It follows a period of sliding and after this a period of stiction again. In dependence on the shape of the beam, the relation between the quasi-static movement and the present coefficient of static friction is analyzed.**

Keywords–Surface detection; vibrissae; friction; mechanical contact; beam; taper.

I. INTRODUCTION

Animals, e.g., rodents and cats collect information about the environment in various ways. They could transduce stimulus of light and sound as well as tactile signals. While light and sound are related to eyes and ears, tactile signals are recorded by tactile hairs. The tactile stimulus represents information about the distance to an object, as well as information about the shape and the surface of the object. The capability of the somatosensory system, including, i.a., the vibrissa, of rodents etc. is high and allows to fulfill the mentioned functions excellent. The concept of a vibrissa is already adapted in several technical devices like sensor systems [1]–[3] or robots [4]–[7]. But, the majority of existing concepts could only differ between different surface textures. The task to detect and classify a surface texture with a technical, vibrissa like sensor is still challenging.

The present work focuses on the theoretical, mechanical background of surface texture detection. Section II gives a brief summary about the morphology of a vibrissa, the biological view of surface texture detection and different mechanical approaches concerning this topic. The details of the used mechanical model are introduced in Section III. The results of the numerical simulation are discussed in Section IV and Section V contains an evaluation of the current state together with an outlook.

II. STATE OF THE ART

There are different types of vibrissae, e.g., the carpal vibrissae are located at the paws and the mystacial vibrissae around the snout of the animal [8]. Because this study concentrates on mystacial vibrissae, the general term *vibrissa* is used for this kind in this paper.

The base of a vibrissa is embedded in the follicle-sinus complex. The follicle-sinus complex is a sophisticated structure that includes, i.a. muscles, mechanoreceptors and elastical tissue. It enables an active movement and control of the vibrissa. The vibrissa itself is characterized by various properties. From in- to outside, there are three layers of different thickness and material properties. The outer layer is covered with scales. Starting from the base of the vibrissa, its diameter gets smaller. In comparison to the length of the vibrissa, the diameter is much smaller. Along the complete length of the vibrissa there is a natural (unstressed) pre-curvature [9]. With the combination of the follicle sinus complex and the vibrissa, the animal could extract information about the distance, the shape and the surface texture while an object is scanned [10].

The authors of [11] and [12] focus on the behavior of the animal while surface texture detection. Using the example of a rat, it is reported that if the vibrissae get into contact with an object respectively surface, the rat will attempt to minimize the deformation of the vibrissae by changing the position of its head. Out of this state, the rat starts to move its head, following a special motion pattern. The authors of [13] observed that the rat repeats the scan three to five times.

There are different hypothesizes how the animals transduce the surface properties via a tactile stimulus into meaningful information. The *vibrissa resonance hypothesis* relates the frequency of a vibrissa to a vibration that is, e.g., caused by surface roughness while the vibrissa is swept along the surface [14]. Analyzing a simillar idea, the authors of [15] and [16] describe the *kinetic signature hypothesis*. The kinetic signature is a temporal pattern of the vibrissa velocity that contains information about the surface texture. A further theory is formulated in [17]. The authors observed that the frequency and the amplitude of the *Stick–Slip* occurrences vary with different surface textures.

From the mechanical point of view, the theoretical background of these hypotheses is not well analyzed. In [18], the vibrissa is assumed as an *Euler-Bernoulli* beam, with

 ISBN: 978-1-61208-518-0

and without a conical beam shape. This model is limited by linear bending theory and not usable for larger deflections. There is no relation between any surface property and the used theory, only a distinction of surfaces is possible. In [19], a flexible probe represents the vibrissa and a spatial distribution of spaces and gaps of macroscopic size the surface. Analyzing this scenario, by using the finite element method and considering only small deflections of the probe, the varying distances of the spaces and gaps are determined. So, the surface texture is classified by a finite number of distance determinations of macroscopic obstacles, this ignores many effects and do not match with smooth surfaces. Determining forces and moments at the base of the virbissa, the initial contact with an object is analyzed in [20]. In this case, the mechanical model adapts various geometrical properties of a real vibrissa, e.g., it considers a tapered and pre-curvature (stress free) shape. The vibrissa is quasi-statical moved, until is touches the object. This model is advanced in [21], where dynamical properties like damping and effects of inertia are added. But, both versions of the model are formulated as multi-body system and do not analyze any surface properties besides the initial contact. Again, supposing that a surface is a spatial distribution of spaces and gaps surface textures are investiagted in [22]. In comparison to [19], there are several differences: The deformation of the straight, conically shaped Euler-Bernoulli beam is a combination of a large deformation (non-linear theory) due to a quasi-static displacement and a small deformation (linear theory) resulting from dynamical effects. Furthermore, the influence of friction (*Coulomb's Law of friction*) is considered in the contact point. Like in the previous models, a relation between surface properties and mechanical is still missing. Only macroscopic effects caused by the spaces and gaps are analyzed.

The authors of [23] form a *first* approach to analyze the connection between surface texture properties and mechanical reactions of the vibrissa in an complete analytical way. Fig. 1

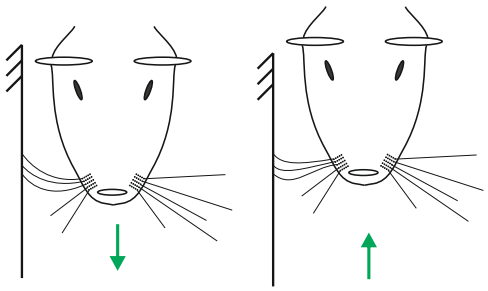

Figure 1. The green arrow represents the direction of motion of the head of the rat.

illustrates the assumed scenario. A rat is scanning a surface by getting in touch with it and moving its head. First, it moves forward (left) and afterwards it starts to move backward (right). The vibrissae are non-stop in touch with the surface, they are sticking to it. While the rat is moving backward the vibrissae gets further deformed, until the coefficient of static friction μ_0 is reached. After this period of sticking, it is sliding until it sticks again. As reaction to the deformation, forces and moments act at the follicle-sinus complex. The follicle-sinus complex is able to encode these stimuli, in a way that the present μ_0 could be determined. Besides that, there is a specific frequency of stick-slip events in dependence on μ_0 if the rat scans a defined length of the surface. This scenario could be adapted for artificial tactile sensor concepts. The following simulations show the described procedure of a surface scan and the influence of a change of the sensor shape with respect to the natural vibrissa morphology.

III. MODELING

Taking over some of the described structural properties in a mechanical model, the following assumptions are done:

- The vibrissa is modeled as an Euler-Bernoulli beam, with respect to large deflections.
- The beam is straight and has a tapered shape.
- The follicle-sinus complex is firstly represented by a clamping.
- The contact between surface and vibrissa is an ideal point contact within the limits of Coulomb's Law of Friction.
- The displacement of the support is quasi-statically.

To simplify the mathematical treatment and to be independent of exact values for, e.g., geometrical parameters or material properties, a nondimensionalization is performed:

$$\text{units:} \quad [\text{length}] = L\,,\ [\text{force}] = \frac{E\,I_{z0}}{L^2}\,,\ [\text{moment}] = \frac{E\,I_{z0}}{L}\,,$$

where L as the length, E as the Young's Modulus, $I_{z0} = \frac{\pi\, d_0^4}{64}$ as the second moment of area and d_0 as the diameter at the base of the beam are the representation of the basic parameters. Using the example of a beam consisting of steel and characterized by the following basic parameters: $E = 2.10 \cdot 10^5\,\text{MPa}$, $d_0 = 5\,\text{mm}$, $L = 100\,\text{mm}$, than the dimensionless force $f = 10.86$ corresponds to a real force F:

$$F = f \cdot [\text{force}] = f \cdot \frac{E\,I_{z0}}{L^2} = 7000\,\text{N}$$

Furthermore, the beam length is given by L with $L = s \cdot [\text{length}]$, whereby s is the arc length:

$$s \in [0, 1]$$

The tapered shape of the beam is defined by the diameter $d(s)$ as function of s, see Fig. 2:

$$d(s) = -\frac{d_0 - \frac{d_0}{\theta}}{L} s + d_0 \tag{1}$$

with the taper factor θ as quotient of d_0 to the diameter of the tip of the beam d_1:

$$\theta := \frac{d_0}{d_1}$$

 ISBN: 978-1-61208-518-0

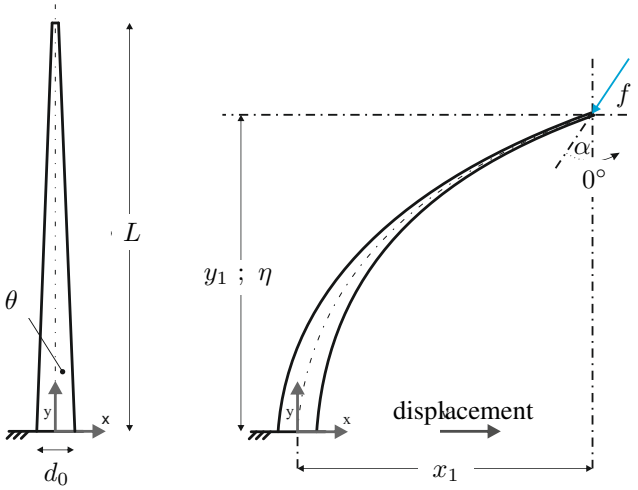

Figure 2. The straight shape of the unloaded tapered beam is shown on the left and the loaded beam on the right.

The position of the tip of the deformed beam is located at (x_1, y_1). The tip is loaded by the force f that is inclined in dependence on the angle of static friction α (counter clockwise counted). The distance between clamping and contact surface is given by η. Using [23] and (1), the set of modeling equations is given by (2):

$$\left.\begin{aligned} x'(s) &= \cos(\varphi(s)) \\ y'(s) &= \sin(\varphi(s)) \\ \varphi'(s) &= \frac{f\,\theta^4}{(\theta\,s-\theta-s)^4}\left[\cos(\alpha)\,(x(s)-x_1)\right. \\ &\qquad \left. +\sin(\alpha)\,(y(s)-y_1)\right] \end{aligned}\right\} \quad (2)$$

with boundary conditions (3):

$$\left.\begin{aligned} x(0) &= x_0 \quad ; \quad x(1) = x_1 \\ y(0) &= 0 \quad ; \quad y(1) = y_1 \\ \varphi(0) &= \frac{\pi}{2} \quad ; \quad \varphi(1) = \varphi_1 \end{aligned}\right\} \quad (3)$$

The derivatives of $x(s)$, $y(s)$ and the slope $\varphi(s)$ results in a non-linear system of differential equations (2) and forms together with the boundary conditions (3) a free boundary value problem with two unknown quantities.

To solve this problem, a *shooting method* is used incorporated into MATLAB R2016a. Starting with a guess for the two initial values for the unknown quantities, the resulting system of equations is solved by the *Runge-Kutta-Method 4th order* using MATLAB function *ode45()* and an optimization process begins. This $2d$-optimization is realized by applying the function *fminsearch()* integrated in MATLAB.

IV. Results & Discussion

Using the mentioned algorithm, different simulations are performed. It is assumed that the beam in the initial state is only loaded by a vertical force. Therefore, α is equal to zero. When the quasi-static footpoint displacement starts, α takes negative values and the frictional force loads the tip of the beam, too. Continuing the movement, the beam gets further deformed. When the maximal stiction force is reached respectively passed, the tip of the beam starts to slip.

The traveled distance between the position of the clamping in the initial state and the last state of stiction gives the maximal footpoint displacement $x_{0_{max}}$. So, this group of different states of deformation of the beam is one period of stiction. Fig. 3 shows the movement of the clamping in positive x-direction, with a step size for the footpoint displacement of $x_0 = 0\,(0.001)\,x_{0_{max}}$ and a fixed distance between surface and clamping of $\eta = 0.85$. For a given $\theta = 2$ and $\mu_0 = 0.4$, $x_{0_{max}}$ is determined. At every footpoint position, the forces and moments at the clamping are determined. For a real application, these reactions will be measured with force and torque sensors. Out of these information, it are possible to determine the μ_0 between sensor and surface.

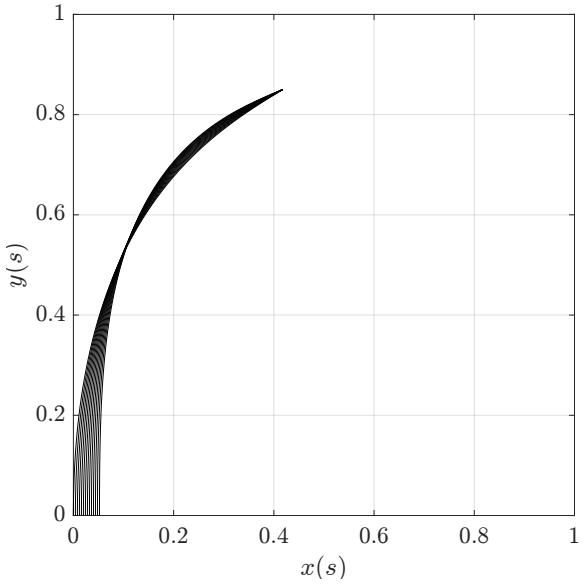

Figure 3. For each position of the clamping the resulting deformed shape of the beam is illustrated.

Like in the previous simulation, the footpoint displacement is set to an increment of $\Delta x_0 = 0.001$ and the distance between surface and clamping to $\eta = 0.85$. The simulation stops after nine stick-slip cycles, see Figs. 4 and 5.

Remark: To describe stick-slip cycles, it is assumed that the period of slipping goes on until the initial condition $\alpha = 0$ is reached again. In this state, a new period of sticking begins.

For each μ_0, a larger θ leads to a larger distance between start and end point of the clamping movement for one period of sticking and also to a stronger deformation of the beam. The comparison of $\mu_0 = 0.3$ and $\mu_0 = 0.4$ indicates a smaller distance of the footpoint displacement and lower deformations of the shape of the beam, for one period of sticking in the case of $\mu_0 = 0.3$.

The distance between start and end point of the footpoint displacement is directly influenced by the values of μ_0 and θ. This influence is important for an artificial sensor. For example, the cylindrical shape ($\theta = 1$) of the beam reacts very sensitive to the footpoint displacement, see Fig. 4a.

 ISBN: 978-1-61208-518-0

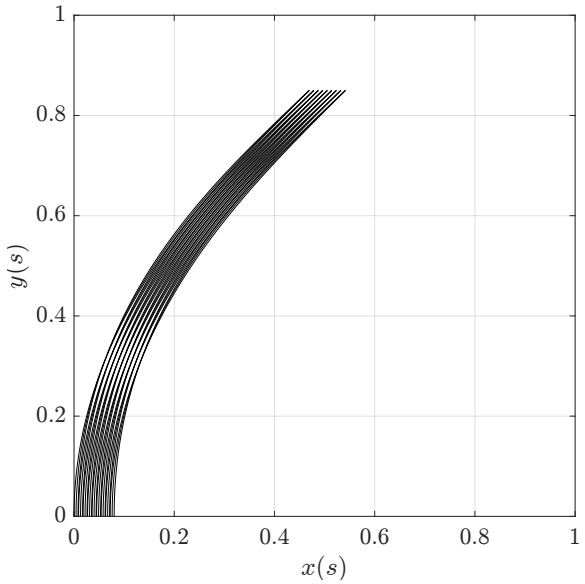

(a) $\theta = 1$

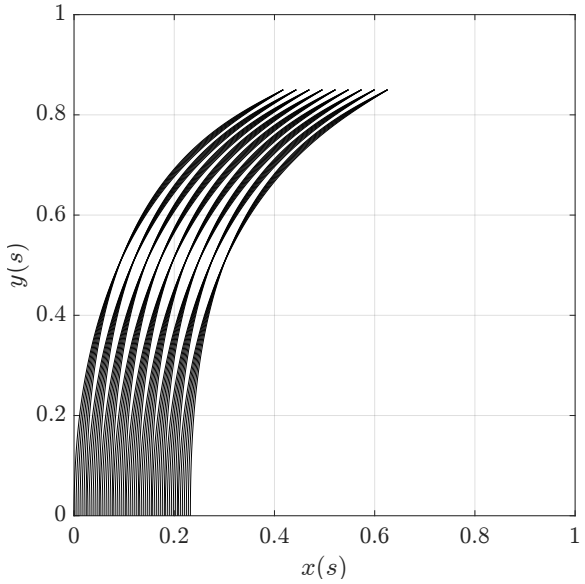

(b) $\theta = 2$

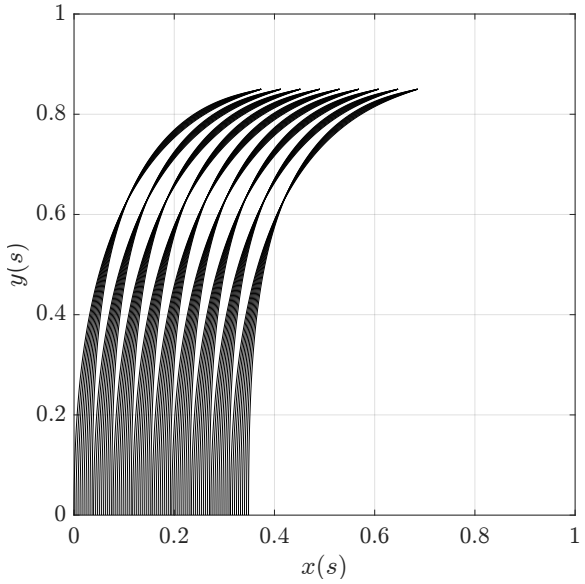

(c) $\theta = 3$

Figure 4. The plots 4a to 4c show the deformed shapes of the beam for different values of θ, a fixed $\mu_0 = 0.3$ and distance between clamping and surface of $\eta = 0.85$.

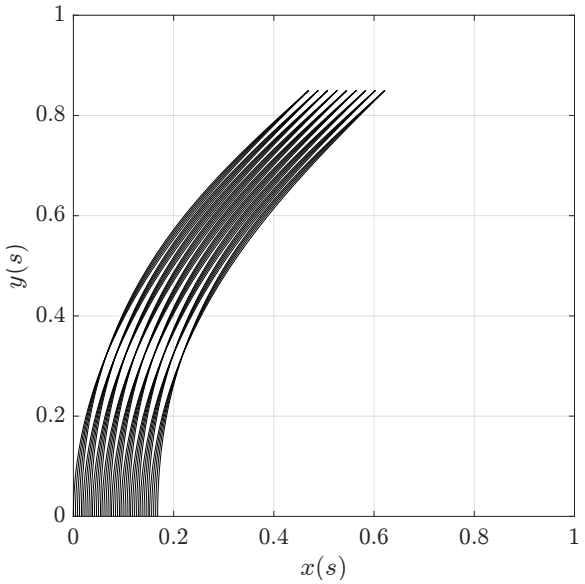

(a) $\theta = 1$

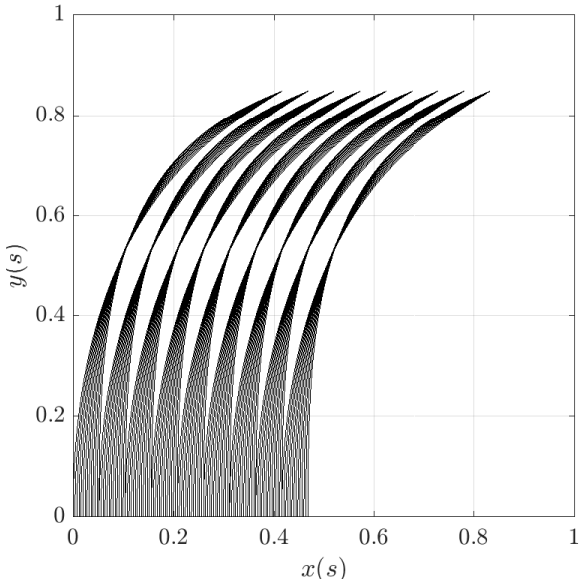

(b) $\theta = 2$

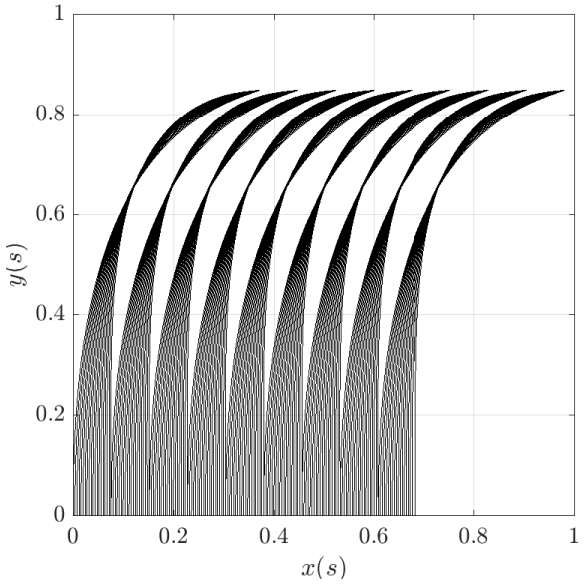

(c) $\theta = 3$

Figure 5. The plots 5a to 5c show the deformed shapes of the beam for different values of θ, a fixed $\mu_0 = 0.4$ and distance between clamping and surface of $\eta = 0.85$.

 ISBN: 978-1-61208-518-0

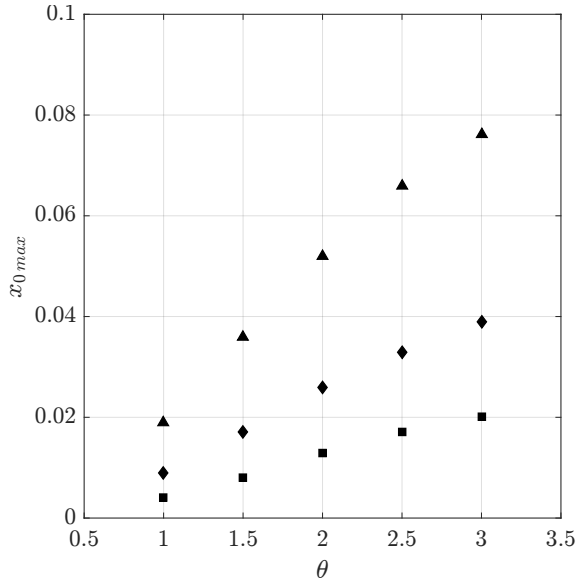

Figure 6. The ordinate shows values for the maximal footpoint displacement of one period of sticking and the abscissa different values of θ.The squares correspond to $\mu_0 = 0.2$, the diamonds to $\mu_0 = 0.3$ and the triangles to $\mu_0 = 0.4$.

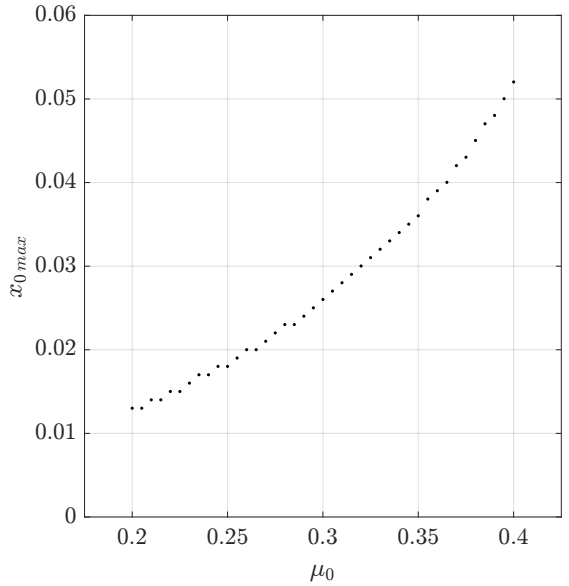

Figure 7. The ordinate shows values for the maximal footpoint displacement of one period of sticking and the abscissa different values of μ_0, with $\theta = 2$.

Already, after a few steps there is a period of sliding. This property is problematic for an artificial sensor because the sensor drive has to be very accurate, else it will be impossible to detect the periods of sticking.

When there is a tapered shape of the beam, this effect is compensated, this is illustrated by the Figs. 4b, 4c and 5b, 5c. A disadvantage of the tapered shape of the beam is the tendency to larger periods of sliding. For an equal quantity of stiction periods, a larger length on a surface has to be scanned. The relation between the maximal displacement of the footpoint $x_{0_{max}}$, θ and μ_0 is summarized for one period of sticking, see Fig. 6. There seems to be a linear correlation between $x_{0_{max}}$ and θ for each value of μ_0. But in contrast, for larger values of μ_0 the effect of a taper shape gets stronger.

This effect is analyzed in Fig. 7. There are different levels of groups of points. Each point is equal to one combination of $x_{0_{max}}$ and μ_0. The different levels are caused by the step size of x_0. The resolution of the step size of x_0 is too large to consider the fine change of the values of μ_0. Based on this result, it is not possible to determine an exact trend of $x_{0_{max}}$ over μ_0, but it seems to be non-linear.

V. Conclusion

The presented mechanical model of a vibrissa includes some typical features of the natural vibrissa, like the conical shape. Also, the approach compromises a model for the contact between vibrissa and touched surface. With in the limits of the Euler-Bernoulli beam theory and Coulomb's Law of Friction, the relations between the tapering factor θ, the maximal footpoint displacement $x_{0_{max}}$, the step size Δx_0 and the coefficient of static friction μ_0 are analyzed by numeric simulations of a quasi-static scenario.

Studying one period of sticking, a larger μ_0 leads to a larger footpoint displacement and stronger deformation of the beam. If the maximal friction force is reached respectively passed, the beam starts to slip. Out of the last state before the slipping starts, the current forces and moments, acting on the support of the beam, can be used to determine the present coefficient of static friction. The influence of θ and μ_0 on stick-slip events is analyzed. For the period of slipping, it is assumed that it goes on until the initial state is reached again. The initial state is characterized by the condition that the angle of static friction α is equal to zero.

A larger θ and μ_0 correspond to longer periods of sticking and sliding. So, for the same quantity of stick-slip events, a longer distance on the contact surface becomes necessary. Also, the total number of steps of the footpoint rises. In short: in dependence on θ a larger μ_0 leads to more stick-slip events.

These findings have to be validated by an experiment in future. Especially, the assumption in the context of the period of slipping is critical. An experiment could also show if there is any relation between other surface properties like roughness, the lay or the waviness.

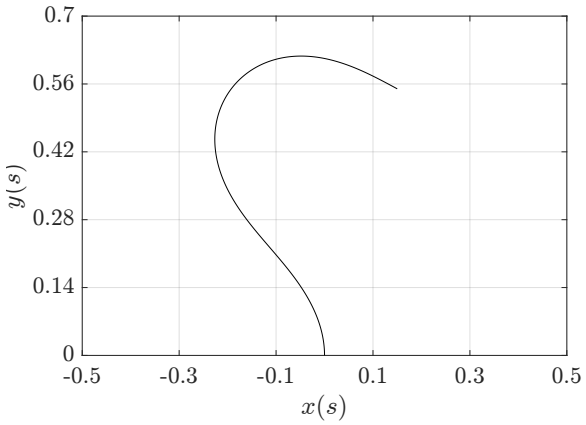

Figure 8. For the values of $x_0 = 0$, $x_1 = 0.15$, $y_1 = 0.55$ and $\theta = 1$ results a deformed shape with a negative value for φ_1.

 ISBN: 978-1-61208-518-0

The mechanical model has to be improved, too. Fig. 8 illustrates the problem. In theory, this result is correct but in reality the shape of the beam penetrates the contact surface. That means the present approach and numeric simulation are not able to analyze every situation in an realistic way. It is necessary to consider a complete contact surface, respectively, line for future simulations.

REFERENCES

[1] M. Lungarella, V. V. Hafner, R. Pfeifer, and H. Yokoi, "An artificial whisker sensors in robotics," in *Proceedings of the IEEE/RSJ International Conference on Intelligent Robots and Systems (IROS) September 30–October 4, 2002, Lausanne, Switzerland*. IEEE, Oct. 2002, pp. 2931–2936, doi: 10.1109/IRDS.2002.1041717.

[2] C. Tuna, J. H. Solomon, D. L. Jones, and M. J. Z. Hartmann, "Object shape recognition with artificial whiskers using tomographic reconstruction," in *Proccedings of theIEEE International Conference on Acoustics, Speech and Signal Processing (ICASSP) March 25–30, 2012, Kyoto, Japan*. IEEE, Mar. 2012, pp. 2537–2540.

[3] F. Ju and S.-F. Ling, "Bioinspired active whisker sensor for robotic vibrissal tactile sensing," *Smart Materials and Structures*, vol. 23, no. 12, pp. 1–9, 2014, doi: 10.1088/0964-1726/23/12/125003.

[4] M. Fend, S. Bovet, H. Yokoi, and R. Pfeifer, "An active artificial whisker array for texture discrimination," in *Proceedings of the IEEE/RSJ International Conference on Intelligent Robots and Systems (IROS) October 27–31, 2003, Las Vegas, USA*. IEEE, Oct. 2003, pp. 1044–1049, doi: 10.1109/IROS.2003.1248782.

[5] D. Kim and R. Möller, "Biomimetic whisker experiments for tactile perception," in *Proceedings of the 3rd International Symposium on Adaptive Motion in Animals and Machines (AMAM) September 25–30, 2005, Ilmenau, Germany*. ISLE, Sep. 2005, pp. 1–7.

[6] S. N'Guyen, P. Pirim, and J.-A. Meyer, *Texture Discrimination with Artificial Whiskers in the Robot-Rat Psikharpax*. Springer Berlin Heidelberg, Jan. 2011, pp. 252–265, Fred, A. et al., Biomedical Engineering Systems and Technologies.

[7] M. J. Pearson, A. G. Pipe, C. Melhuish, B. Mitchinson, and T. J. Prescott, "Whiskerbot: A robotic active touch system modeled on the rat whisker sensory system," *Adaptive Behavior*, vol. 15, no. 3, pp. 223–240, 2007, doi: 10.1177/1059712307082089.

[8] T. Helbig, D. Voges, S. Niederschuh, M. Schmidt, and H. Witte, *Characterizing the Substrate Contact of Carpal Vibrissae of Rats during Locomotion*. Springer International Publishing, Aug. 2014, pp. 399–401, Duff, A. et al., Biomimetic and Biohybrid Systems.

[9] D. Voges et al., "Structural characterization of the whisker system of the rat," *IEEE Sensors Journal*, vol. 12, no. 2, pp. 332–339, 2012, doi: 10.1109/JSEN.2011.2161464.

[10] K. Carl et al., "Characterization of statical properties of rat's whisker system," *IEEE Sensors Journal*, vol. 12, no. 2, pp. 340–349, 2012, doi: 10.1109/JSEN.2011.2114341.

[11] B. Mitchinson, C. J. Martin, R. A. Grant, and T. J. Prescott, "Feedback control in active sensing: rat exploratory whisking is modulated by environmental contact," *Proceedings of the Royal Society B: Biological Sciences*, vol. 274, no. 1613, pp. 1035–1041, 2007, doi: 10.1098/rspb.2006.0347.

[12] R. A. Grant, B. Mitchinson, C. W. Fox, and T. J. Prescott, "Active touch sensing in the rat: Anticipatory and regulatory control of whisker movements during surface exploration," *Journal of Neurophysiology*, vol. 101, no. 2, pp. 862–874, 2009, doi: 10.1152/jn.90783.2008.

[13] G. E. Carvell and D. J. Simons, "Biometric analyses of vibrissal tactile discrimination in the rat," *The Journal of Neuroscience*, vol. 10, no. 8, pp. 2638–2648, 1990.

[14] C. I. Moore and M. L. Andermann, *The Vibrissa Resonance Hypothesis*. CRC Press, 2005, chaper 2, pp. 21–60, Ebner, F., Somatosensory Plasticity.

[15] E. Arabzadeh, E. Zorzin, and M. E. Diamond, "Neuronal encoding of texture in the whisker sensory pathway," *PLoS Biology*, vol. 3, no. (1):e17, pp. 1–11, 2005, doi: 10.1371/journal.pbio.0030017.

[16] J. Hipp et al., "Texture signals in whisker vibrations," *Journal of Neurophysiology*, vol. 95, no. 3, pp. 1792–1799, 2006, doi: 10.1152/jn.01104.2005.

[17] J. Wolfe et al., "Texture coding in the rat whisker system: Slip-stick versus differential resonance," *PLoS Biology*, vol. 6, no. (8):e215, pp. 1–17, 2008, doi: 10.1371/journal.pbio.0060215.

[18] A. E. Schultz, J. H. Solomon, M. A. Peshkin, and M. J. Z. Hartmann, "Multifunctional whisker arrays for distance detection, terrain mapping, and object feature extraction," in *Proccedings of the IEEE International Conference on Robotics and Automation (ICRA) April 18–22, 2005, Barcelona, Spain*. IEEE, Apr. 2005, pp. 2588–2593, doi: 10.1109/ROBOT.2005.1570503.

[19] A. Vaziri, R. A. Jenks, A.-R. Boloori, and G. B. Stanley, "Flexible probes for characterizing surface topology: From biology to technology," *Experimental Mechanics*, vol. 47, no. 3, pp. 417–425, 2007, doi: 10.1007/s11340-007-9046-8.

[20] B. W. Quist and M. J. Z. Hartmann, "Mechanical signals at the base of a rat vibrissa: the effect of intrinsic vibrissa curvature and implications for tactile exploration," *Journal of Neurophysiology*, vol. 107, no. 9, pp. 2298–2312, 2012, doi: 10.1152/jn.00372.2011.

[21] B. W. Quist, V. Seghete, L. A. Huet, T. D. Murphey, and M. J. Z. Hartmann, "Modeling forces and moments at the base of a rat vibrissa during noncontact whisking and whisking against an object," *The Journal of Neuroscience*, vol. 34, no. 30, pp. 9828–9844, 2014, doi: 10.1523/JNEUROSCI.1707-12.2014.

[22] Y. Boubenec, L. N. Claverie, D. E. Shulz, and G. Debrégeas, "An amplitude modulation/demodulation scheme for whisker-based texture perception," *The Journal of Neuroscience*, vol. 34, no. 33, pp. 10 832–10 843, 2014, doi: 10.1523/JNEUROSCI.0534-14.2014.

[23] J. Steigenberger, C. Behn, and C. Will, "Mathematical model of vibrissae for surface texture detection," 2015, preprint No. M 15/03 19 pages, Technische Universität Ilmenau, Germany.

 ISBN: 978-1-61208-518-0